Identification of residual nano-scale foulant material on stainless steel using atomic force microscopy after clean in place

Phinney, David; Goode, Kylee; Fryer, Peter; Heldman, Dennis; Bakalis, Serafeim

DOI:
10.1016/j.jfoodeng.2017.06.019

Document Version
Peer reviewed version

Citation for published version (Harvard):
Phinney, D, Goode, K, Fryer, P, Heldman, D & Bakalis, S 2017, 'Identification of residual nano-scale foulant material on stainless steel using atomic force microscopy after clean in place', *Journal of Food Engineering*. https://doi.org/10.1016/j.jfoodeng.2017.06.019

Identification of residual nano-scale foulant material on stainless steel using atomic force microscopy after clean in place

David M. Phinney, Kylee Goode, Peter J. Fryer, Dennis Heldman, Serafim Bakalis

PII: S0260-8774(17)30265-0

DOI: 10.1016/j.jfoodeng.2017.06.019

Reference: JFOE 8924

To appear in: *Journal of Food Engineering*

Please cite this article as: David M. Phinney, Kylee Goode, Peter J. Fryer, Dennis Heldman, Serafim Bakalis, Identification of residual nano-scale foulant material on stainless steel using atomic force microscopy after clean in place, *Journal of Food Engineering* (2017), doi: 10.1016/j.jfoodeng.2017.06.019

Title

Identification of residual nano-scale foulant material on stainless steel using atomic force microscopy after clean in place

Authors

David M. Phinney[a,b], Phinney.14@osu.edu (Corresponding author)

Kylee Goode[b], k.r.goode@bham.ac.uk

Peter J Fryer[b], p.j.fryer@bham.ac.uk

Dennis Heldman[a,c], heldman.20@osu.edu

Serafim Bakalis[b], s.bakalis@bham.ac.uk

[a]The Ohio State University, Department of Food Science & Technology.

2015 Fyffe Ct., Columbus OH 43210. USA

[b]University of Birmingham, School of Chemical Engineering

Edgbaston, Birmingham, West Midlands, B15 2TT. UK

[c]The Ohio State University, Department of Food, Agriculture and Environmental Science

590 Woody Hayes Drive, Columbus, OH 43210. USA

Abstract

During clean-in-place (CIP), solutions are pumped through process equipment to remove soils having adverse effects on production. In order to validate reductions in CIP inputs, foulants need to be detectable and quantifiable on smaller scales than current industrial practices. In this study, fluorescent microscopy was used for quantifying macroscopic cleanliness of a soiled stainless steel coupon after CIP. An asymptotic model was used to describe the removal of soil as a function of the coupon exposure time and cleaning solution temperature. From these models, cleaning parameters were determined and used to generate coupons predicted to be 99.0 and 99.9% clean. This cleanliness was verified using atomic force microscopy (AFM). AFM identified foulant on the order of 5 μm^2 on a 1.0 x 10^4 μm^2 area. AFM showed cleanliness ranging from 99.41 to 99.94 %. Differences between predicted and actual cleanliness suggest a change in cleaning mechanism at different scales.

Key words

Clean in place; atomic force microscopy; fluorescence microscopy; protein fouling; thermal processing

1. Introduction

The process of cleaning in place (CIP) is typically achieved by pumping large volumes of cleaning solution (most commonly detergents or strong bases) through process pipelines and sprayed on tank walls to remove residual deposits from contact surfaces (Heldman and Lund, 2007). There are variations on CIP steps but all of them would contain a "cleaning" step. During the cleaning step (which usually comes after a pre-rinse of the system with water) detergent solutions are pumped through the system to remove strongly adhered deposits. Several CIP variables surrounding the detergent solutions have been investigated in the past for their significance in effective cleaning during CIP (Fickak et al., 2011; Gillham et al., 1999; Jeurnink and Brinkman, 1994). Recently, the area of CIP has developed interest from industrial perspectives because reduction in water inputs to cleaning operations can reduce total plant water consumption significantly (Tiwari et al., 2016). To this effect, researchers have specifically begun to investigate reductions in water, chemical, electrical energy and time consumption during CIP. Reductions in total inputs to a CIP operation must maintain hygiene after a CIP operation is complete. Furthermore, despite various advances in CIP research and technology, industries often use a visual check to validate CIP protocols (Forsyth et al., 2006). Therefore, advances in defining a clean contact surface on smaller scales must be developed in an effort to better quantify the effect of reducing CIP inputs (water, chemicals and energy). Without better defining "how clean is clean," clean process technology advances are limited (Bakeev, 2010; Jones et al., 2012).

In cleaning research, the size of deposit is an important variable to define, especially when comparing deposits of different magnitudes. 'Length' scales to describe the size of deposits in cleaning and fouling research have been previously presented (Akhtar et al., 2010). The presented scale describes fouling layers ranging from millimeter lengths (e.g. residual thick material in tanks or lines after processing) down to nanometer lengths (e.g. molecules on a contact surface). There is a large range of

foulant materials ranging between the molecular level (very small) and thick films (very large). Included in this range is the "meso" scale sized foulant materials. The Meso scale, although not perfectly defined, represents a large majority of the body of cleaning research. Examples of meso scale foulants in food manufacturing include heat exchanger burn on and mineral build up. Recent research has correlated the meso scale adherence of foulant at the nano scale. Akhtar et al., (2010) investigated the force required to remove a foulant adhered to various substrates on the meso scale using micro-manipulation techniques, and subsequently compared that to the nano scale force of adherence using atomic force microscopy (AFM). The authors found that there are correlations between meso and nano force requirements when correcting for surface area. Similarly, the research completed in this paper uses a fluorescence microscopy technique to create predictive cleaning models on the meso scale and compare those models to predicted cleanliness at the nano scale.

Two types of forces have been previously described during the process of cleaning (Liu et al., 2006). *Cohesive* forces are those that bond the foulant to itself, where *adhesive* forces bond the foulant to the surface. Many cases have shown the cleaning process begins as primarily cohesive removal and ends being entirely adhesive (Midelet and Carpentier, 2004; Palabiyik et al., 2014). Conditions that determine which set of forces control the process, and how this can be altered, are largely unknown. Furthermore, these two phases of foulant removal (adhesive and cohesive cleaning) predominate differently on different sizes of foulant. For example large deposits (cm length scale) will primarily undergo cohesive removal initially where small deposits (nm length scale) require primarily adhesive forces. In the nano length scale, during cleaning, the removal of deposits can be considered entirely adhesive (Bobe et al., 2007; Okorn-schmidt et al., 2014). The research performed here focuses on the application of instrumentation developed for nano technology to investigate what is happening on a molecular level towards the completion of a cleaning process.

In cleaning research, the method for quantifying hygiene level is clearly defined and governed by the scale at which the investigation is pertinent. (Cole et al., (2010) investigated removal of large deposits by completely filling an industrial pipe section with toothpaste and applying water to remove the toothpaste. This scale is on the order of grams of deposit per area, or meters when discussing the length scale of foulant previously defined. In this case, Cole et al., (2010) used turbidity and electrical conductivity of the solution leaving the pipe as indicators of the removal of toothpaste from the pipeline during a rinse with pure water (i.e. no detergents or other cleaning agents) where the solution was directly pumped to the drain. Determining cleaning time at this scale is governed by the detection limits of the instrumentation used and the removal of nanometer length sized deposits may have been undetectable by the instrument response (Klahre and Flemming, 2000; Van Asselt et al., 2002). The research performed in this manner, i.e. research that primarily focuses on large visual deposits, can be considered macro-foulant research.

Other research has evaluated extremely sensitive instrumentation for detecting deposit formation and removal on the nano lengths scale. Chen et al., (2010) and Favrat et al., (2012) used a quartz crystal microbalance (QCM) which allows for real time determination of nano-gram amounts of deposit on various substrates determined by changes in vibrational properties of the substrate itself. The QCM technology provides knowledge of deposition and removal of foulants at the molecular level but is also limited in range, which does not allow it to form a commercially relevant thickness of foulant on the substrate.

A large body of academic literature focuses on the meso length scale. For example, whey protein gels have been used to study the mass transfer of detergent in to a model foulant (Fickak et al., 2011; Mercadé-Prieto et al., 2008; Mercadé-Prieto and Chen, 2006) at mm to micron scale . The passage of chemicals in to the foulant deposit is the first necessary step in removing deposits which remain after

a water rinse. This concept is transferrable to the deposit on the nano length scale, because nano-scale deposits of dairy based foulants need chemical modification prior to removal. This chemical modification is governed by the rate of diffusion of cleaning agent in to deposit and therefore represents a mass transfer step prior to either dissolution of the foulant or physical removal (peeling) of the deposit (Changani et al., 1997; Fryer et al., 2006).

Deposits in the hundreds of nano grams of foulant per square centimeter represent the micro length scale as well as that which can be considered primarily adhesive removal. Fan et al., (2015) studied the removal of a dairy type foulant from the surface of commercial pipelines. Residual deposit levels, after a rinse cycle was complete, were determined by extracting foulant residues from the inner pipe surface in to a solution and subsequently determining the protein content of that solution. Here, alkaline solutions were used to dissolve the remaining dairy based deposit in to solution and said solutions protein level was used as an indicator for residual deposit in the pipe section. Limitations with the degree of detection in this method are directly tied to the volume of extraction fluid and extraction process. For example, too little extraction fluid used runs the risk of not removing 100 % of the remaining foulant while too much fluid dilutes the concentration of protein in the extraction and renders it below the detection limit of the assay.

It was the goal of this research to develop an analytical methodology to investigate “visual cleanliness” using fluorescent microscopy and subsequently compare cleaning rates to the level of hygiene on a nano-level using atomic force microscopy (AFM). AFM has been used previously to characterize adhesion forces (Fang et al., 2000; Handojo et al., 2009). The focus of the research presented in this paper was the use nano instrumentation to detect nano level residual foulant material on food contact surfaces, subsequently employing methods to quantify the nano-deposit using image processing. Multiple approaches to the detection and quantification of nano deposits using atomic force

131 microscopy were explored. This work differs from the majority of industrial cleaning research by
132 identifying the deposit itself *in situ* opposed to looking at the indicators of foulant in a cleaning solution.

133 ## 2. Materials and methods

134 ### 2.1 Substrate characterization

135 Square 2.54 x 2.54 cm stainless steel (316L type) coupons were used as the model food contact
136 substrate in this study. Coupons were polished to a mirror finish using automotive grade sand papers
137 and polishing compound. Coupons were analyzed using atomic force microscopy (AFM) in tapping mode
138 to characterize surface properties prior to use in experimentaiton. A Nanowizard II AFM (JPK
139 Instruments AG, Berlin, Germany) was used for all AFM analyses performed. For initial roughness
140 determination it was imperative that the coupons surface be clean. Because "clean" is focal point of the
141 research, it is important to note – in detail – this method. To achieve "clean" coupons, coupons (after
142 polishing) were cleaned using 2.0 % (wt./wt.) NaOH and distilled water at 80 °C under agitation for 1
143 hour. Coupons were removed and rinsed with 1.0 % (vol./vol.) aqueous solutions of HCl. Coupons were
144 subsequently soaked in hexane for 5 minutes and then acetone for another 5 minutes. All solvents were
145 HPLC grade solvents purchased from Fisher Scientific LLC. After removal from acetone, samples were
146 allowed to air dry and were then analyzed using the AFM. A 100 x 100 µm area was scanned with a 512 x
147 512 resolution. Cross sectional analysis was completed using JPKSPM Image Software. Surface
148 roughness (R_a), root mean square roughness (R_q) and peak to valley roughness (R_t) was determined for
149 all coupons used in this study. Results for initial surface characteristics are: R_a = 95 nm (±17 nm), R_q =
150 131(±26 nm) and R_t = 744 (±142 nm). After AFM analysis, the coupons showed sufficient similarity in
151 roughness to justify their use in the present study.

152 ### 2.2 Foulant deposition

153 Whey protein concentrate (WPC) solutions were used as the model foulant to be adhered to the
154 stainless steel substrate. 10 % (wt./wt.) solutions of WPC (CARBALEC 35, Carbery, Ballineen, Co Cork,
155 Ireland) were created by blending WPC powder with distilled water at room temperature while being
156 stirred with a magnetic stir bar on a stir plate for an hour or until homogenous. Significant effort was
157 made to minimize aeration of the solution during the mixing/hydration stage to minimize foaming and
158 denaturation of the proteins in solution. 1 ml of the WPC solution was then pipetted on to the stainless
159 steel coupon and the coupon was then heated at 75 °C for 1 hour on a hot plate. This time and
160 temperature profile was used because it minimized bubble formation (because it was well below 100 °C)
161 and allowed gelation of the solution. The heating process induced gelation as well as dehydrated the
162 foulant on to the coupon surface. The coupons were then cooled to room temperature before exposure
163 to clean in place conditions.

164 Consistency of the initial foulant deposit was tested by checking the increase in coupon mass
165 after heating. Since 1 ml of 10 % (wt./wt.) solution was applied to each coupon, the increase in mass
166 should be around 0.1 g (solids in 1 ml). Results showed mass was increased 0.114 (±0.012) g.

167 2.3 Cleaning procedure

168 0.5 % (wt./wt.) solutions of NaOH were used as the clean in place (CIP) solution during this
169 study. 1000 g of solution was added to a 2 L (D = 6.25 cm) beaker and was stirred using a 4.5 cm stir bar
170 at 300 rotations per minute (RPM). The clean in place (CIP) variable of interest in this study was the
171 temperature of the caustic solution. Temperature and RPM was monitored and controlled by using
172 Adwin Scientific IKA heated stir plate (Adwin Scientific Direct, Schaumburg, Illinois, USA). Coupons were
173 exposed to 40, 55 and 70 °C cleaning solutions for varying periods of time by suspending the coupon in
174 the CIP solution using an attached string for exposure and removal to the solution. The coupon was
175 lowered so that the center face of the coupon was 0.06 m below the surface of the cleaning solution

with the coupon's back against the beaker wall. The temperature range was selected to ensure significant separation of cleaning rates between the treatments.

To evaluate the flow conditions of the benchtop vessel, two approaches were utilized. Firstly, the impeller Reynolds number (N_{Re_i}) was used to calculate turbulence level at each temperature condition. N_{Re_i} (Eq. 1) is calculated as;

$$N_{Re_i} = \frac{\rho N D^2}{\mu} \quad (1)$$

Where ρ is the density of water at T, N is rotations per second of the stir bar, D is the diameter of the stir bar and μ is the viscosity of water at T. Values for density and viscosity of water were obtained from the National Institute of Standards and Technology (NIST) database. The turbulence value for a stirred vessel begins at N_{Re} = 10,000 (Sinnott, 1999). The corresponding N_{Re} values for 40, 55 and 70 °C are 15,400, 19,800 and 24,500 respectively. All of which correspond to a turbulent flow condition which would be targeted during CIP. Although the N_{Re_i} represents turbulence at the tip of the impeller, with all other conditions held constant (vessel size, volume of solution and rotational speed) it can be used to correlate the relative turbulence changes between conditions.

The second approach at characterizing the flow conditions in the benchtop vessel was to create a computational fluid dynamics (CFD) model of the design and extract various flow parameters from the simulation. COMSOL Multiphysics (Version 5.2a, Palo Alto, California, USA) was used to create the physical design of the system in a digital space. For the CFD model, the turbulent k-ε flow was used with the rotating machinery physics module to simulate the beaker stir bar combination. Average shear rate over the coupon surface was extracted using the rmspf.sr expression. Shear rate over the coupon surface for 40, 55 and 70 °C was determined to be 62.3, 74.5 and 85.7 s^{-1} respectively. The CFD model was also used to calculate the average velocity (by integration of the velocity profile distribution) from

198 the surface of the coupon, to 0.5 cm away from the surface. The average velocity was determined for
199 40, 55 and 70 °C to be 16.9, 17.3 and 17.5 cms^{-1} respectively. The slight changes in average velocity are
200 due to the changes in viscosity at the various temperatures in the mixing tank model.

201 It is important to clarify that the purpose of the research was not specifically to characterize the
202 effects of temperature on cleaning, rather the development of cleaning models at each temperature to
203 extend to the AFM evaluations. Exposure times at each temperature were selected by first visually
204 determining the time of removal foulant deposit under each condition. That time of (complete visual)
205 removal was then divided evenly in to 6-7 time points between initial exposure and the endpoint. After
206 removal from the cleaning solution, coupons were rinsed with ~25 ml of distilled water and heated at 75
207 °C on a hot plate for 30 minutes to drive off excess moisture and secure residual foulant material to the
208 coupon. After the CIP procedure, coupons were analyzed using fluorescent and atomic force
209 microscopy.

210 2.4 Fluorescent microscopy

211 2.4.1 Instrumentation and image acquisition

212 The aim of this study was to characterize the removal of a foulant from a “visual” cleanliness
213 method. In order to complete such an investigation, analytical methods for determining visual
214 cleanliness had to be developed. Because dairy proteins naturally fluoresce, fluorescent microscopy was
215 used as a surrogate to create an analytical method for visual cleanliness. Fluorescent images ware taken
216 using a Leica digital microscope with a fluorescent light generator and digital filterset to look for
217 fluorescent light in the 410-420 nm range (Moro et al., 2001). Images were acquired using a XIMEA
218 MR285-MU (Ximea Corp., Golden, CO 80401, USA) at 10 times magnification using µManager software
219 as the camera controlling software. At this magnification, approximately 90% of the 2.54 x 2.54 cm
220 coupon was imaged, creating a macroscopic image of the coupon is its entirety. Significant effort was

made to control all aspects of image acquisitions and microscope adjustments to ensure identical image parameters for each acquisition. The 8-bit images were taken and subsequently analyzed using ImageJ (Schneider et al., 2012).

2.4.2 Clean vs. dirty

Cleanliness was determined by using the intensity of pixels in the 8-bit color space (256 shades of grey). The histogram of color scores for a dirty coupon was achieved by imaging 6 coupons which had been fouled by the aforementioned foulant deposition process. The fluorescent images were acquired after a period of 30 s of exposure to fluorescent light to allow for stabilization of the photo bleaching. Dirty coupons were evaluated in an identical manner but the coupon was cleaned using the same solvent cleaning process from the substrate characterization process. Typical distribution frequency of pixels for each of these can be seen in Fig. 1.

Fig. 1 shows a clear separation between the clean and dirty coupons at an approximate color value of 41 to 51. Distributions of “clean” and “soiled” coupons were produced from 6 replicates and the grey value separating those distributions was determined (by evaluating the minimum of the sum of the two normal distributions) to be 45. Therefore, any pixel with a color score of 45 or above was considered to fluoresce bright enough that it would be considered “dirty” and any pixel with a score less than 45 was considered to be “clean.” There is a limitation in using fluorescence in that the intensity of whey proteins decays with time (photo bleaching). Classifying pixels as soiled vs. clean after fluorescent stabilization overcomes this issue. After the initial exponential decay (30 s) in fluorescent intensity (due to photo bleaching) residue proteins still have significant intensity to have them identify as being “dirty.”

This evaluation method created a binary response from individual pixels in each image. Therefore, a complex image of various pixel intensities was converted in to only clean and dirty pixels. ImageJ was used to analyze the image and the percent area clean was calculated using Eq. 2.

$$A\%\ clean = \left(1 - \frac{n_{\geq 45}}{N}\right) x\ 100\% \quad (2)$$

Where *A %* is the percentage of area that is clean, $n_{>45}$ is the sum total of the number of pixels in the image with a color score of 45 or above and *N* represents the total number of pixels in the image. A pictographic representation of the conversion of images from original image to percent clean can be seen in Fig. 2.

2.4.3 Mathematical modeling

Fluorescent microscopy results were used to develop predictive models for the removal of the foulant from the stainless steel coupons. To model the removal, a sigmoidal function was selected as the fundamental equation. This was chosen for the following reasons;

(i) The method of cleaning used is based on color intensity rather than the thickness of foulant in that pixel. Therefore, the process was predicted to have a larger induction cleaning period where the foulant would be swelling and dissolving in to the cleaning solution (Mercadé-Prieto and Chen, 2006). During this swelling phase, this image analysis method would return a 100 % "dirty" response, even if some amount of layer 'thickness' had been removed.

(ii) Secondly, if the swelling and dissolution of the foulant was evenly distributed over the coupon surface, then once "clean" pixels were exposed they would increase in number at some rate as a function of time.

(iii) Lastly, there would have to be an asymptotic decay towards 100% "clean" pixel, as that is the only end point.

Therefore, the sigmoidal growth model first proposed by Gompertz (Gompertz, 1825) was used in this study. This model has been used and modified extensively throughout academic research primarily in microbiological studies (Belda-Galbis et al., 2014; Chatterjee et al., 2014; Hossain et al., 2016). Although

seldom used in swelling/dissolution research such as this, the model has been successful in fitting the various stages of microbial growth. The model used in this study can create sigmoidal curves which are symmetric around a central value using Eq. 3.

$$y = y_{max}\ e^{-e^{-k(t-t_m)}} \quad (3)$$

Here y_{max} represents the maximum cleanliness value attainable by the model, t is the continuous variable of time, k represents the rate at which the sigmoid approaches its upper and lower asymptote and t_m represents the time value at which $\frac{y}{y_{max}}$ is equal to e^{-1}. In this case y_{max} is equal to 100 % because that is the maximum level of cleanliness so it is removed from the model. Therefore there are only two parameter estimates needed to predict these sigmoidal functions from the fluorescent data; k and t_m.

2.4.4 Experimental design & statistical analysis

The fluorescent microscopy investigation was completed using a completely randomized design which included 3 temperatures and 6 levels of time for the 70 °C condition, 7 levels of time for the 55 °C condition and 8 levels of time for the 40 °C condition. PROC NLIN in SAS 9.4 (SAS Institute, Cary, North Carolina, USA) was used to estimate model parameters (k and t_m) for the sigmoidal modeling of each temperature. The standard error of the parameter estimates were used as goodness of fit parameters.

2.5 Atomic force microcopy

2.5.1 Time point selection method

Cleaning rates based on the fluorescent microscopy results were used to determine the cleaning time variables needed for the atomic force microscopy analysis portion of the research. Two predicted cleaning times were calculated from Equation 1 for each of the three temperatures (40, 55 and 70 °C). The two cleaning times were predicted by calculating the time at which the coupons would be predicted

to be 99.0 and 99.9 percent clean. This created 6 variables for the AFM analysis (3 temperatures at 2 predicted cleanliness levels). This method was selected to investigate if the visual cleaning rate could be translated and continued in to the non-visual scale. If that case was true, then each of the AFM images for each level of predicted cleanliness would appear insignificantly different, *and* the difference in cleanliness within a temperature between 99.0 and 99.9% clean would be distinguishable.

Samples for AFM analysis were fouled and subsequently exposed to CIP conditions for the predetermined times. Samples were then rinsed with distilled water and washed with room temperature (~23 °C) 1 % HCl to simulate an acid rinse which comes after the mid rinse step during the CIP operation. This HCl rinse is meant to remove any mineral based deposits which may originate from the fouling method, ensuring that any residual deposits detected could be considered a primarily proteinaceous based matrix. After the HCl rinse, coupons were again rinsed with ~25 ml of distilled water and dried on a 75 °C hot plate for approximately 30 minutes.

2.5.2 Surface topography

Surface topography of samples was evaluated using AFM contact mode with a silicon nitride AFM tip with 0.32 N/m force constant (Part # PN-TR-TL-Au-20 A, Nanoworld AG, Neuchâtel, Switzerland). Tips were calibrated for spring constant and resonance frequency each session. 100 x 100 µm areas were scanned with a 512 x 512 resolution and a tip speed of approximately 100 µm/s. Images were processed using JPKSPM Data Processing Software. Images were corrected to have fixed height/color values for direct comparison of the images and for further image analysis.

2.5.3 Force mapping

Samples identified to have residual deposits from the surface topography were evaluated using a force mapping approach. The goal of force mapping was to correlate non-uniformities in surface

topographies with non-uniformities in attraction and repulsion forces between the tip and the surface. Confirmation of distinguishability between "clean" stainless steel and residual nano-deposits using force mapping could verify the existence of residual deposits even when the topography failed to identify it. For instance, if a small deposit was to reside between two peaks of the substrate, the region would appear smooth and clean from a topography evaluation. But if the force of integration responded differently to fouled regions, this method could identify the deposit in this scenario.

Force mapped samples were evaluated using the tipless version of the AFM tip used in the surface topography evaluation. A 30 nm diameter stainless steel sphere (part # SSMMS-7.8 27-31um 0.2g, Copheric LLC, Santa Barbara, CA, USA) was adhered to the cantilever using two part epoxy and the AFM controls. Again, 100 x 100 µm areas were mapped using 512 x 512 resolutions similar to what was used in the surface topography evaluation.

3 Results & discussion

3.1 Fluorescent microscopy

Visual cleanliness determined by fluorescent microscopy results are presented in Fig. 3. Overlaid on the raw data are the Gompertz sigmoidal models. Parameter estimates and standard errors from each of these models are presented in Table 1. We can see that as the temperature of the cleaning solution increases that the k value increases while t_m decreases. It has been well studied that increased temperatures increases the cleaning rate (Fan et al., 2015; Gillham et al., 1999). The goal of this research was to develop a method using fluorescent microscopy as a surrogate for visual cleanliness, not specifically to study the effect of temperature. Simeone et al., (2016) used fluorescence imaging and ultrasonic evaluation during the removal of chocolate sauce from stainless steel. Here, fluorescent intensity was well correlated with foulant thickness and a real time model for removal of the chocolate sauce were identified. The analytical methods in this paper are different than Simeone et al., (2016)

because thickness of the deposit could not be correlated with fluorescent intensity due to photo bleaching of whey proteins. Therefore, this research used a binary clean/dirty approach for images of fouled surfaces.

Table 1: Table of the parameter estimates needed to create the fitted sigmoidal models on the fluorescent data (solid lines on Figure 2). The plus/minus refers to the standard error on the parameter estimate generated from SAS 9.4 PROC NLIN.

Temp (°C)	k (s^{-1})	t_m(s)
40	0.064 ±0.01	92.0 ±1.1
55	0.25 ±0.05	49.1 ±0.4
70	0.41 ±0.03	32.7 ±0.2

The Gompertz sigmoidal growth model tended to fit the data quite well across the whole set with an average percent standard error of 9.76 % and 1.7 % for k and t_m respectively. The more interesting area of the sigmoid occurs at or near the value of t_m, where the error between replicates can be quite large. For example, after a 90 s exposure time at 40 °C the coupon cleanliness ranged (in the statistical sense of 'range') from 25 to 49 % clean between the three replicates. This error would then decrease purely from the assumption about the model once the process heads towards 100% clean. This suggests that at the levels beyond the detectable range of the fluorescent microscope that the errors decrease. It is important to understand that in this particular sigmoid model, the larger statistical distribution of raw values (i.e. "percent clean") is highest towards t_m because this is the exponential portion of the model. Therefore, small differences in experimental error (say one extra second of exposure time from experimental error) has a large effect on the response. This is handled by the use of statistics to predict t_m, and even though the deviation of raw values is large at this value of t_m, the standard error is quite small. Similar methodologies for data processing are found in logarithmic transformation to data that is not identically distributed within the variables.

The use of direct fluorescent microscopy (opposed to say ATP fluorescence) on a commercial active heating surface, which has been processing dairy based, products is largely unknown. Future investigations should focus on how a foulant formed under commercial processing conditions responds to fluorescent exposure and how to intensify and quantify this foulant.

3.2 Atomic force microscopy

3.2.1 Surface topography

Using the results from Table 1 in the fluorescent microscopy portion of the research, the exposure times needed to achieve 2 "levels of cleanliness" (99.0 and 99.9 %) for each temperature were calculated using Equation 2. Table 2 shows these exposure times for the 6 variables (3 temperature and 2 levels of cleanliness) used for the surface topography and the force mapping completed using atomic force microscopy (AFM).

Table 2: Calculated exposure times for generation of samples to be analyzed using AFM. Values were calculated using the parameter estimates in Table 2 and solving for time in Equation 2.

	Predicted exposure time (s)	
Temperature (°C)	99.0 % clean	99.9 % clean
40	165	200
55	65	100
70	45	60

Single image results for the surface topographies of each of these samples are presented in Fig. 4. Here we can see when compared to the clean stainless steel surface, many of the samples have localized peaks which are up to 350 nm in height. These localized collections of peaks represent residual nano-foulant material on the surface which is not detectable through fluorescent microscopy because of its detection threshold being larger than AFM. Some interesting trends in residual deposit can be seen in the surface topographies. If we look across the 90.0 % clean coupons, samples are almost

372 indistinguishable from one another. The foulant islands in each of these maps are very similar in shape,
373 size and quantity. It is important to reiterate that these samples were exposed to cleaning solution for
374 very different period of times. The 40, 55 and 70 °C samples were exposed to 165, 65 and 45 s
375 respectively (as noted in Table 3). The results suggest that at the 99.0 % cleanliness level predicted
376 through fluorescence microscopy the removal rate parameters (k and t_m) hold true.

377 In contrast, when the topographies across the 99.9 % cleanliness level are compared, results
378 appear different. Although each time point here was predicated to have the same cleanliness, the
379 residual deposits on the surface increase with a decrease in temperature. Specifically, when looking at
380 the difference in surface topography between 99.0 and 99.9% clean at the CIP temperature of 40 °C, no
381 distinguishable difference in surface topographies can be identified, despite the predicted difference.
382 This suggests an alternative cleaning mechanism at the nano level during cleaning and removal of tightly
383 adhered deposits. Future work in this area should focus in investigating how the model changes as a
384 function of the scale at which CIP is working on.

385 Quantification of nano-deposits at this level proves significantly difficult. The variation in surface
386 topography of the stainless steel itself proves challenging to subtract out from the topographic images.
387 A Matlab^{tm} code (V.R2013a, Mathworks inc., Massachusetts, USA) was developed using image
388 processing tools to convert AFM images to quantifiable values. The image extracted from JPKSPM
389 software was first converted to a black and white image and then converted to a binary image using a
390 threshold of 0.9. The thresholding value here needed to be set large enough that the peaks of the
391 stainless steel surface itself are removed. The binary image was processed in to morphological
392 structures using Matlab 'Strel' function to identify 'disk' objects in the binary image. The 'disks' were
393 then identified as foulant and percent cleanliness of each sample in the 100 x 100 µm area using Eq. 1

was estimated. Fig. 5 shows all the steps in this image process to extract quantitative data from the AFM topographical results. Table 3 shows the average results (n = 2) of cleanliness values for each condition.

Table 3: Results for the percent cleanliness of the AFM samples analyzed by surface topography. Plus/minus values represent standard deviation (n=2).

	Cleanliness (%)	
Temperature (°C)	99.0 % clean	99.9 % clean
40	99.4 ±0.36	99.7 ±0.12
55	99.8 ±0.06	99.9 ±0.05
70	99.4 ±0.70	99.9 ±0.06

This particular method of quantifying residual foulant is analogous to the optical method completed in the fluorescence microscopy portion of the study. As another form of a 2-dimensional analysis, it can only detect how much surface area has foulant on it but not how tall said foulant is. Further analysis using the AFM data height mapping should be the next step in quantification of nano-foulants on surface in a 3-dimensional approach.

3.2.2 Force mapping

Several force maps were taken in an effort to further identify indicators of residual foulant materials on the stainless steel surface. Interaction between the custom AFM tip and a clean sample (cleaned using the aforementioned solvent method in section 2.4.2) were analyzed first to create baseline attraction and repulsion measurements. It was found that the custom AFM tip consistently had an adhesion force (approximately 1 nN) to the clean stainless steel surface. The adhesion force was defined as the minimum deflection of the AFM tip's cantilever when removed from contact with the surface. This phenomenon was investigated further using samples which were first identified to have residual deposits by analyzing topography. Although preliminary, results showed that there was a

similarity in “clean” areas of the partially fouled coupons and the force interaction on a deposit did not show the adhesion force. Fig. 6 shows the 3-d projection of a force map and the extraction of two plots of vertical deflection as the tip is retracted. Here we can see when the AFM tip retracts from what is seemingly a clean area of the coupon (point A), an approximately 2 nN adhesion force is observed. When the identical map is extracted on the foulant region (point B) there is seemingly no adhesion force observed. This attribute is seemingly quite consistent across various points within the AFM force maps. Validating changes in interaction forces (adhesion forces or otherwise) will help to identify residual deposits when surface topography fails. Future investigation in the area of detection and quantification of nano-foulants should focus in this area.

5. Conclusions

The current investigation used advanced analytical techniques commonly used in nano materials science and applied them to hygienic design in food process engineering. Specifically, fluorescence microscopy was used to determine the effect of temperature on a dairy type model foulant on stainless steel during exposure to cleaning solution for various times. A Gompertz asymptote model was parameterized and fit to the fluorescence data to generate predictive cleaning equations for visual cleanliness. The predictive equations were used to create samples for analysis using atomic force microscopy (AFM). The AFM was able to characterize residual nano-foulants on the order of 5 μm^2 as well as identify the lack of fit of the nano-deposit removal when compared to the visually clean model. Interaction forces between a custom AFM tip and stainless steel with and without deposit was investigated. Strong adhesion forces seem to predominate when the tip interacted with clean areas and where areas with residual foulant showed none. The work completed here shows significant advances in the detection and quantification of residual material on food contact surfaces. Advances in this area are necessary for advancing validation procedures for clean in place operations on a commercial scale. The

437 results show the “next level” of detection and quantification of residual foulant material on food contact
438 surfaces, setting a stage for advanced analytical methods for certifying cleanliness of food contact
439 surfaces.

440 Acknowledgements

441 The authors would like to thank the Society of the Chemical Industry for their Seligman APV Fellowship
442 which allowed for the collaborative research completed in this study.

443 References

444 Akhtar, N., Bowen, J., Asteriadou, K., Robbins, P.T., Zhang, Z., Fryer, P.J., 2010. Matching the nano- to the
445 meso-scale: Measuring deposit-surface interactions with atomic force microscopy and
446 micromanipulation. Food Bioprod. Process. 88, 341–348. doi:10.1016/j.fbp.2010.08.006

447 Bakeev, K.A., 2010. Process analytical technology: spectroscopic tools and implementation strategies for
448 the chemical and pharmaceutical industries. John Wiley & Sons.

449 Belda-Galbis, C.M., Pina-Perez, M.C., Espinosa, J., Marco-Celdran, A., Martinez, A., Rodrigo, D., 2014. Use
450 of the modified Gompertz equation to assess the Stevia rebaudiana Bertoni antilisterial kinetics.
451 Food Microbiol. 38, 56–61. doi:10.1016/j.fm.2013.08.009

452 Bobe, U., Hoffman, J., Sommer, K., Beck, U., Reiners, G., 2007. Adhesion - where cleaning starts 18, S36-
453 39. doi:10.1016/j.tifs.2006.10.019

454 Changani, S.D., Belmar-Beiny, M.T., Fryer, P.J., 1997. Engineering and chemical factors associated with
455 fouling and cleaning in milk processing. Exp. Therm. Fluid Sci. 14, 392–406. doi:10.1016/S0894-
456 1777(96)00141-0

457 Chatterjee, T., Chatterjee, B.K., Majumdar, D., Chakrabarti, P., 2014. Antibacterial effect of silver

458 nanoparticles and the modeling of bacterial growth kinetics using a modified Gompertz model.
459 Biochim. Biophys. Acta 1850, 299–306. doi:10.1016/j.bbagen.2014.10.022

460 Chen, M.-Y., Chen, M.-J., Lee, P.-F., Cheng, L.-H., Huang, L.-J., Lai, C.-H., Huang, K.-H., 2010. Towards real-
461 time observation of conditioning film and early biofilm formation under laminar flow conditions
462 using a quartz crystal microbalance. Biochem. Eng. J. 53, 121–130. doi:10.1016/j.bej.2010.10.003

463 Cole, P.A., Asteriadou, K., Robbins, P.T., Owen, E.G., Montague, G.A., Fryer, P.J., 2010. Comparison of
464 cleaning of toothpaste from surfaces and pilot scale pipework. Food Bioprod. Process. 88, 392–
465 400. doi:10.1016/j.fbp.2010.08.008

466 Fan, M., Phinney, D.M., Heldman, D.R., 2015. Effectiveness of rinse water during in-place cleaning of
467 stainless steel pipe lines. J. Food Sci. 80, E1490–E1497. doi:10.1111/1750-3841.12914

468 Fang, H.H., Chan, K.Y., Xu, L.C., 2000. Quantification of bacterial adhesion forces using atomic force
469 microscopy (AFM). J. Microbiol. Methods 40, 89–97. doi:10.1016/S0167-7012(99)00137-2

470 Favrat, O., Gavoille, J., Aleya, L., Monteil, G., 2012. Real Time Study of Detergent Concentration
471 Influence on Solid Fatty Acid Film Removal Processes. J. Surfactants Deterg. 1–7.
472 doi:10.1007/s11743-012-1383-7

473 Fickak, A., Al-Raisi, A., Chen, X.D., 2011. Effect of whey protein concentration on the fouling and cleaning
474 of a heat transfer surface. J. Food Eng. 104, 323–331. doi:10.1016/j.jfoodeng.2010.11.004

475 Forsyth, R.J., Hartman, J.L., Nostrand, V. Van, 2006. Risk management assessment of visible residue
476 limits in cleaning validation. Pharm. Technol. 30, 104–114.

477 Fryer, P.J., Christian, G.K., Liu, W., 2006. How hygiene happens: Physics and chemistry of cleaning. Int. J.
478 Dairy Technol. 59, 76–84. doi:10.1111/j.1471-0307.2006.00249.x

479 Gillham, C.R., Fryer, P.J., Hasting, A.P.M., Wilson, D.I., 1999. Cleaning-in-Place of whey protein fouling
480 deposits. Food Bioprod. Process. 77, 127–136. doi:10.1205/096030899532420

481 Gompertz, B., 1825. On the nature of the function expressive of the law of human mortality, and on a
482 new mode of determining the value of life contingencies. Philos. Trans. R. Soc. London 115, 513–
483 583.

484 Handojo, A., Zhai, Y., Frankel, G., Pascall, M.A., 2009. Measurement of adhesion strengths between
485 various milk products on glass surfaces using contact angle measurement and atomic force
486 microscopy. J. Food Eng. 92, 305–311. doi:10.1016/j.jfoodeng.2008.11.018

487 Heldman, D.R., Lund, D.B., 2007. Handbook of Food Engineering, 2nd ed. CRC Press, Taylor & Francis
488 Group. Boca Raton, FL.

489 Hossain, F., Follett, P., Dang Vu, K., Harich, M., Salmieri, S., Lacroix, M., 2016. Evidence for synergistic
490 activity of plant-derived essential oils against fungal pathogens of food. Food Microbiol. 53, 24–30.
491 doi:10.1016/j.fm.2015.08.006

492 Jeurnink, T.J.M., Brinkman, D.W., 1994. The cleaning of heat exchangers and evaporators after
493 processing milk or whey. Int. Dairy J. 4, 347–368. doi:10.1016/0958-6946(94)90031-0

494 Jones, I., Cullen, P.J., Greene, A., 2012. Using PAT to support the transition from cleaning process
495 validation to continued cleaning process verification. J. Valid. Technol. 18.1, 50–56.

496 Klahre, J., Flemming, H.C., 2000. Monitoring of biofouling in papermill process waters. Water Res. 34,
497 3657–3665.

498 Liu, W., Fryer, P.J., Zhang, Z., Zhao, Q., Liu, Y., 2006. Identification of cohesive and adhesive effects in the
499 cleaning of food fouling deposits. Innov. Food Sci. Emerg. Technol. 7, 263–269.

500 doi:10.1016/j.ifset.2006.02.006

501 Mercadé-Prieto, R., Chen, X.D., 2006. Dissolution of whey protein concentrate gels in alkali. AIChE J. 52,
502 792–803. doi:10.1002/aic.10639

503 Mercadé-Prieto, R., Paterson, W.R., Chen, X.D., Wilson, D.I., 2008. Diffusion of NaOH into a protein gel.
504 Chem. Eng. Sci. 63, 2763–2772. doi:10.1016/j.ces.2008.02.029

505 Midelet, G., Carpentier, B., 2004. Impact of cleaning and disinfection agents on biofilm structure and on
506 microbial transfer to a solid model food * 262–270. doi:10.1111/j.1365-2672.2004.02296.x

507 Moro, A., Gatti, C., Delorenzi, N., 2001. Hydrophobicity of whey protein concentrates measured by
508 fluorescence quenching and its relation with surface functional properties. J. Agric. Food Chem. 49,
509 4784–4789. doi:10.1021/jf001132e

510 Okorn-schmidt, H.F., Holsteyns, F., Lippert, A., Mui, D., Kawaguchi, M., Lechner, C., Frommhold, P.E.,
511 Nowak, T., Reuter, F., Piqu, B., Cair, C., Mettin, R., 2014. Particle Cleaning Technologies to Meet
512 Advanced Semiconductor Device Process Requirements 3, 3069–3080. doi:10.1149/2.011401jss

513 Palabiyik, I., Olunloyo, B., Fryer, P.J., Robbins, P.T., 2014. Flow regimes in the emptying of pipes filled
514 with a Herschel-Bulkley fluid. Chem. Eng. Res. Des. 92, 2201–2212.
515 doi:10.1016/j.cherd.2014.01.001

516 Schneider, C. a, Rasband, W.S., Eliceiri, K.W., 2012. NIH Image to ImageJ: 25 years of image analysis. Nat.
517 Methods 9, 671–675. doi:10.1038/nmeth.2089

518 Simeone, A., Watson, N., Sterritt, I., Woolley, E., 2016. A Multi-sensor Approach for Fouling Level
519 Assessment in Clean-in-place Processes. Procedia CIRP 55, 134–139.
520 doi:10.1016/j.procir.2016.07.023

521 Sinnott, R.K., 1999. Coulson & Richardson's Chemical Engineering, Volume 6: Chemical Engineering
522 Design (4th ed.). Elsevier Butterworth Heinemann.

523 Tiwari, S., Behera, C.R., Srinivasan, B., 2016. Simulation and experimental studies to enhance water
524 reuse and reclamation in India's largest dairy industry. J. Environ. Chem. Eng. 4, 605–616.
525 doi:10.1016/j.jece.2015.12.001

526 Van Asselt, A.J., Van Houwelingen, G., Te Giffel, M.C., 2002. Monitoring System for Improving Cleaning
527 Efficiency of Cleaning-in-Place Processes in Dairy Environments. Food Bioprod. Process. 80, 276–
528 280. doi:10.1205/096030802321154772

529

Figure 1: Color distributions of clean (A) and dirty (B) coupons imaged under fluorescent microscopy. Error bars show standard deviation of samples (n=6).

Figure 2: Comparison of the original images acquired on the fluorescent microscope (top row) the same image after conversion to the clean/dirty image (bottom row). Red pixels in the image represent pixels with a color score higher than 45 and are therefore considered dirty.

Figure 3: Results from the fluorescent microscopy cleaning investigation with sigmoidal model fits (lines) overlaid on the raw data (squares). Each square represents the average of 3 randomized experiments with standard deviations presented as error bars. Dashed lines represent the 95 % confidence interval around each prediction model.

Figure 4: Results from the surface topography investigation using atomic force microscopy.

Figure 5: Figure 5: From left to right is; (1) the original AFM image from JPKSPM analysis, (2) the image converted to black and white, (3) the image converted in to a binary image and (4) the Matlab^{tm} 'strel/disk' identification in the binary image.

Figure 6: 3-dimnesional projection of a height tract on 100 x 100 µm area (top) which was analyzed using AFM force mapping. The vertical deflection of the AFM cantilever during retraction at two points (bottom) are separately plotted.

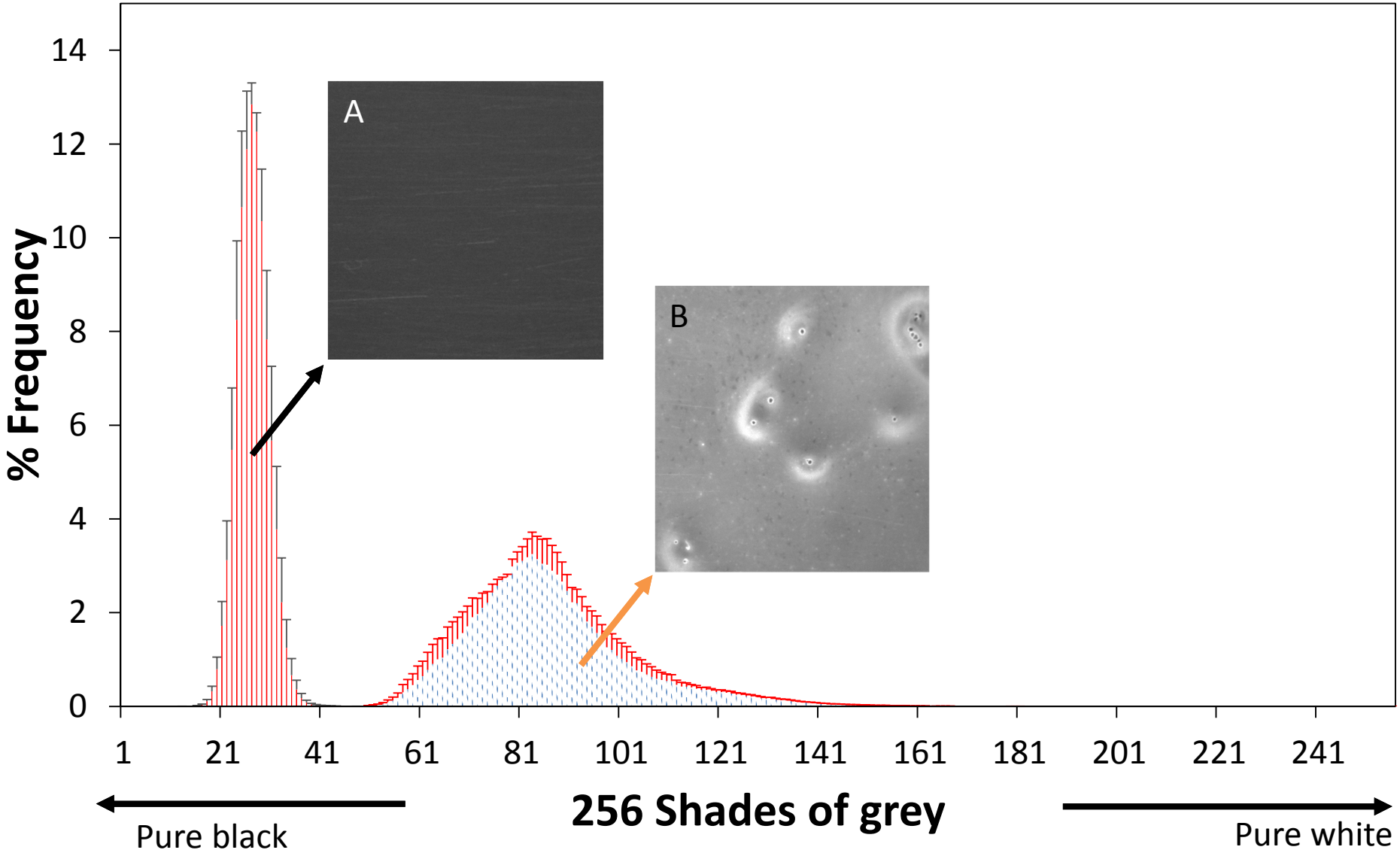

Figure 1: Color distributions of clean (A) and dirty (B) coupons imaged under fluorescent microscopy. Error bars show standard deviation of samples (n=6).

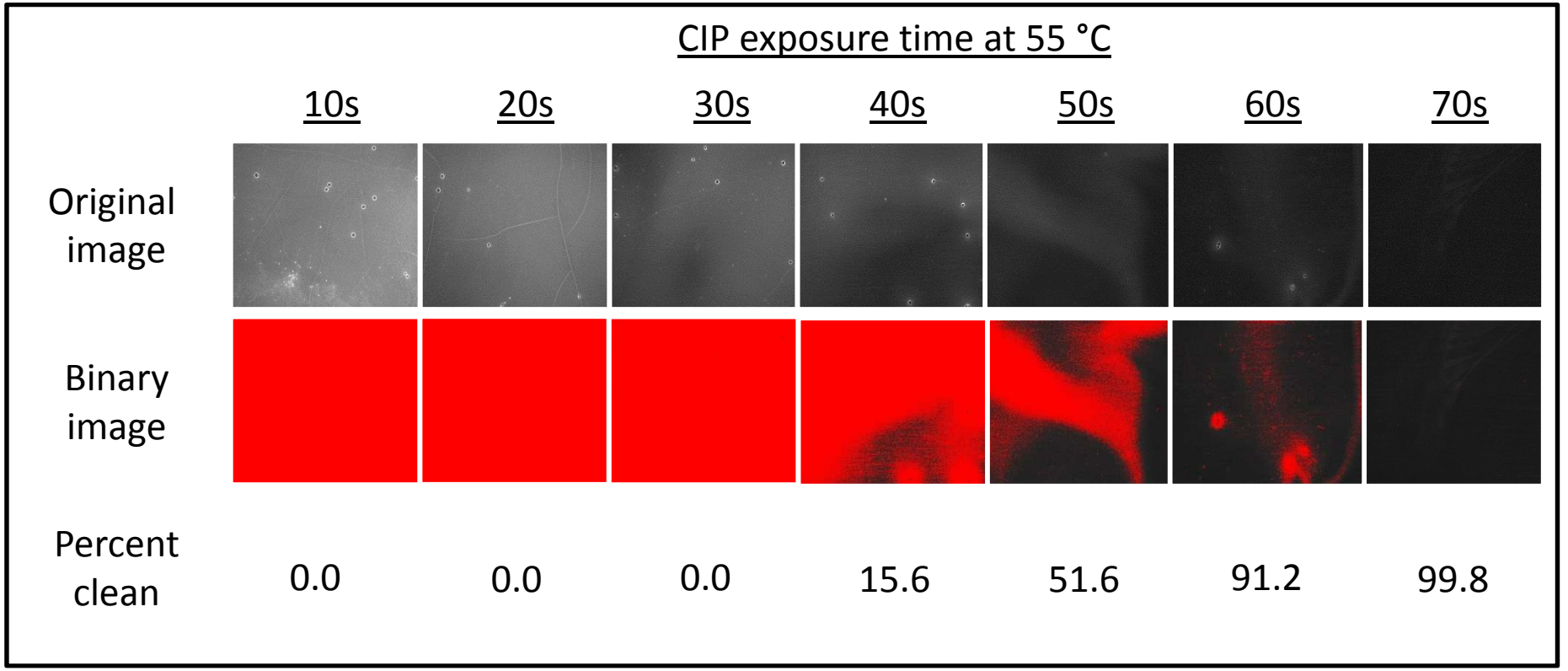

Figure 2: Comparison of the original images acquired on the fluorescent microscope (top row) the same image after conversion to the clean/dirty image (bottom row). Red pixels in the image represent pixels with a color score higher than 45 and are therefore considered dirty.

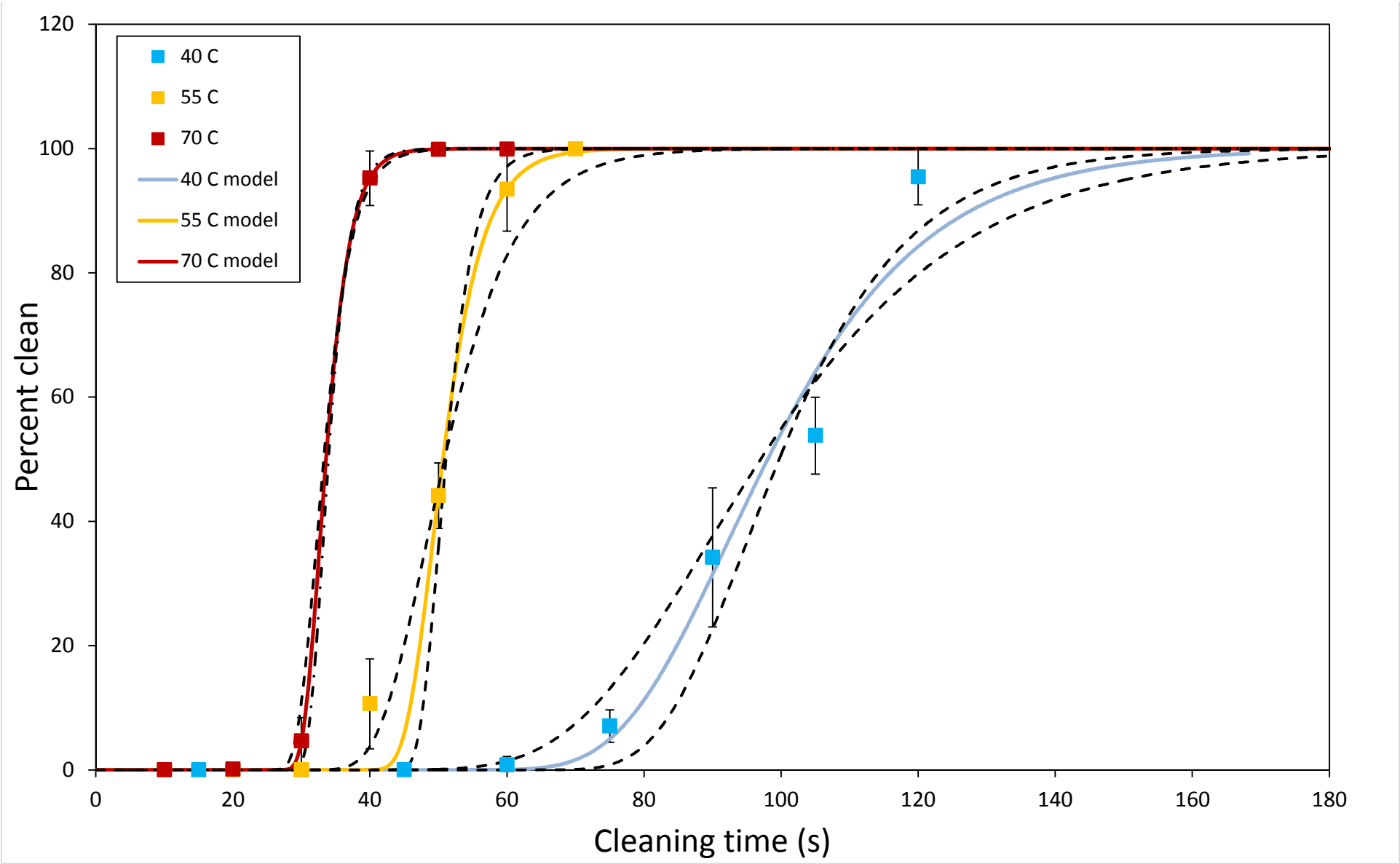

Figure 3: Results from the fluorescent microscopy cleaning investigation with sigmoidal model fits (lines) overlaid on the raw data (squares). Each square represents the average of 3 randomized experiments with standard deviations presented as error bars. Dashed lines represent the 95 % confidence interval around each prediction model.

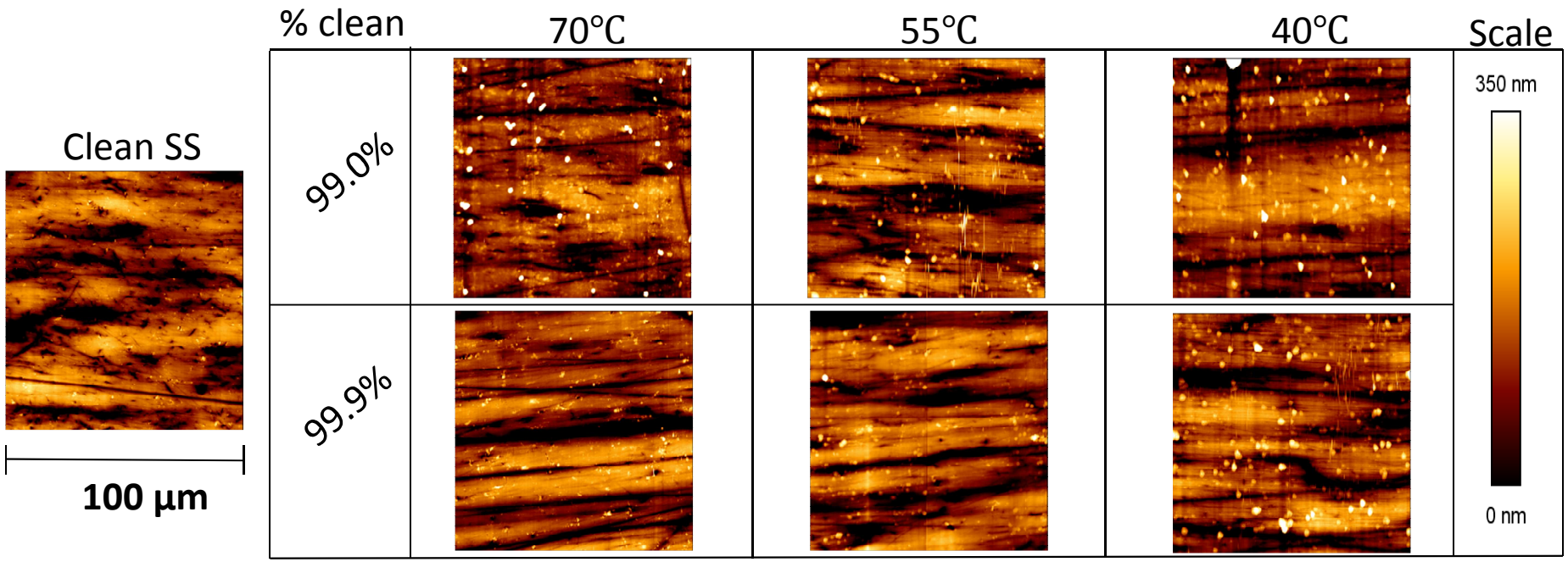

Figure 4: Results from the surface topography investigation using atomic force microscopy.

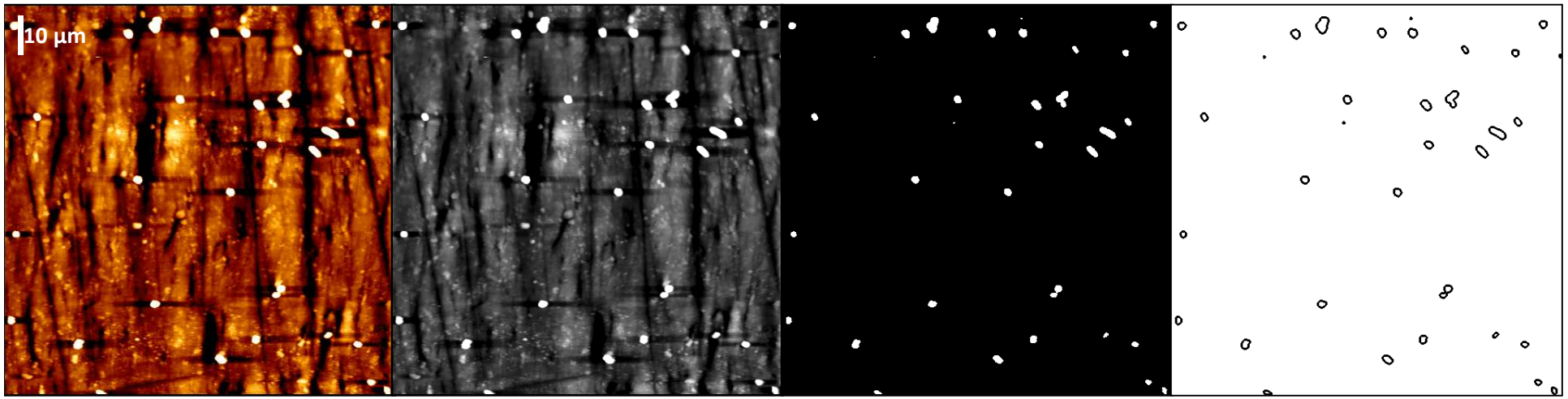

Figure 5: From left to right is; (1) the original AFM image from JPKSPM analysis, (2) the image converted to black and white, (3) the image converted in to a binary image and (4) the Matlab^{tm} 'strel/disk' identification in the binary image.

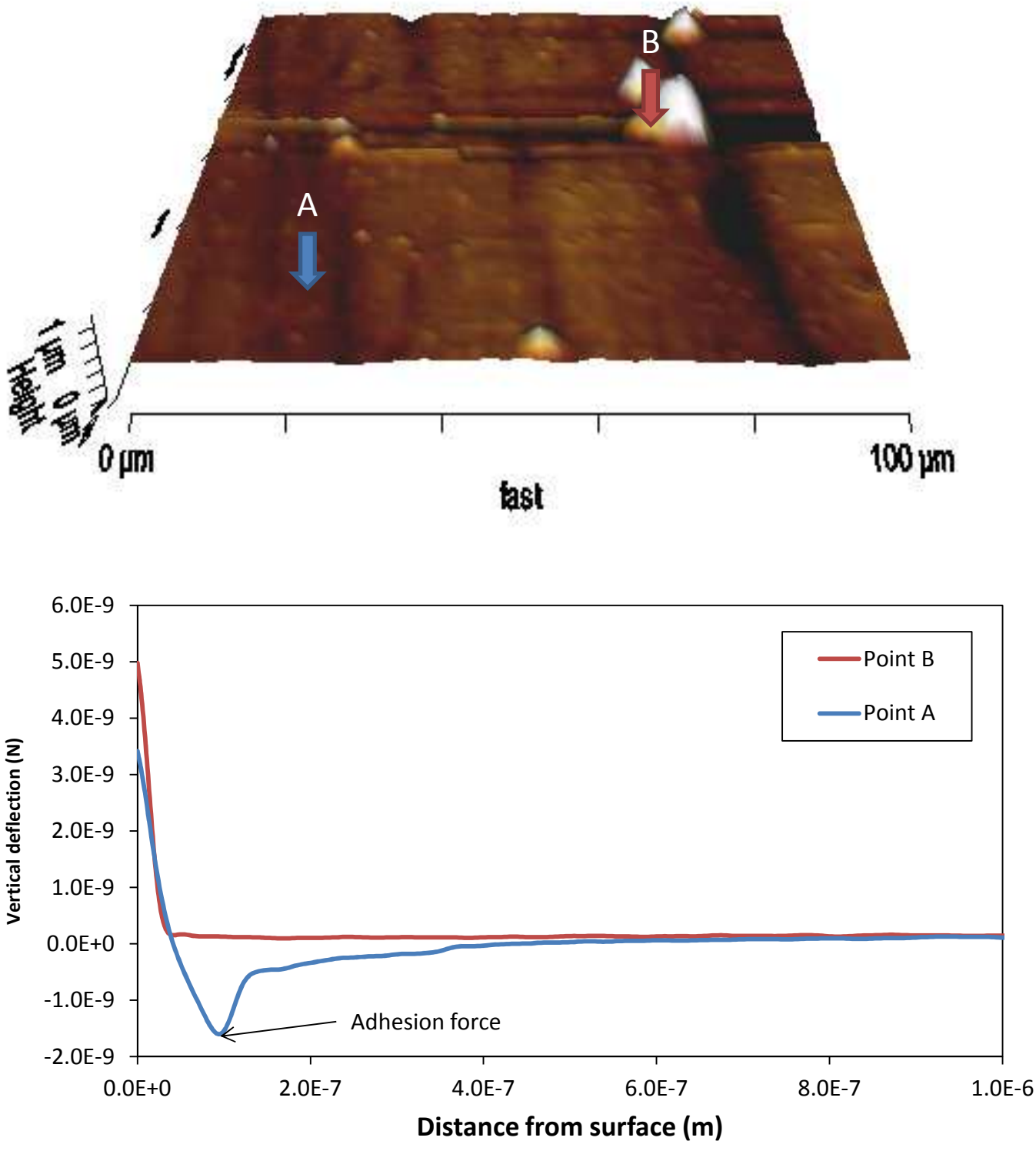

Figure 6: 3-dimnesional projection of a height tract on 100 x 100 µm area (top) which was analyzed using AFM force mapping. The vertical deflection of the AFM cantilever during retraction at two points (bottom) are separately plotted.

Highlights

- Fluorescence microscopy quantified visual surface cleanliness
- Visual cleanliness fit a sigmoidal cleaning model for whey protein deposits
- Atomic force microscopy was able to identify invisible deposits
- Invisible deposits as small as 5 μm^2 could be identified